International Journal of Rock Mechanics & Mining Sciences 98 (2017) 67–77

Contents lists available at ScienceDirect

International Journal of Rock Mechanics & Mining Sciences

journal homepage: www.elsevier.com/locate/ijrmms

An efficient algorithm for simulating grout propagation in 2D discrete fracture networks

S. Mohajerani[a], A. Baghbanan[b], G. Wang[c,*], S.F. Forouhandeh[d]

[a] Department of Mining Engineering, Petroleum and Geophysics, Shahrood University of Technology, Shahrood, Iran
[b] Department of Mining Engineering, Isfahan University of Technology, Isfahan, Iran
[c] Department of Civil and Environmental Engineering, Hong Kong University of Science and Technology, Hong Kong
[d] Mathematical Department, Shahrood University of Technology, Shahrood, Iran

ARTICLE INFO

Keywords:
GroutIUT[2D]
EGFP algorithm
Groutability
Sensitivity analyses
DFN

ABSTRACT

This study is aimed at developing a computationally efficient algorithm to simulate the grout fluid propagation by generalizing the recently developed Explicit Grout Forehead Pressure algorithm to two-dimensional discrete fracture networks. A computer program is developed by using an innovative recursive scheme to track the paths of grout propagation within the fractures, and the results can be visualized using a graphic interface. The efficiency and accuracy of the algorithm is successfully validated using two series of laboratory tests. Finally, sensitivity analyses are conducted to study the influence of key parameters, including initial pressure, grout fluid density, grout viscosity and operation time, on the grout propagation for both dry and saturated in-situ conditions. The study demonstrates that the existence of pore fluid inside the fractured medium can significantly decrease the propagation area. Some other less studied factors are also investigated, such as time-dependent hardening of the grout viscosity, initial yield stress of the grout fluid and rheology properties of the in-situ pore fluid. These factors are also found to be important for improving efficiency of the grout operation.

1. Introduction

The existence of discontinuities is the most important reason for decreasing strength and the increasing permeability of rock masses in comparison with the intact rock. Considering the effect of discontinuities is very crucial in the large scale rock engineering projects such as mining, civil, hydrogeology and petroleum reservoir engineering. Grouting operation is one of the most effective techniques for ground improvement, and plays a specific role in increasing the strength of rock foundations, stabilizing rock slopes, underground openings and decreasing water inflow into the underground and surface excavations.

To date, many research works have been focused on developing more accurate methods to predict the grout take, i.e., amount of raw material needed for grouting, and grout propagation in fractured rock mass based on initial parameters, such as geometrical parameters of rock fractures, rheological parameters of grout fluid and operational parameters of grouting. Empirical methods[1–4] in predicting the groutability of rock masses usually cannot provide desired precision. Therefore, analytical or numerical methods for predicting groutability were developed. For example, Wang et al.[5] applied a pipe network modelling to calculate fluid flow in a three-dimensional fractured medium. Ericsson et al.[6] used a numerical modelling to study the grouting in a two-dimensional lattice network of fractures. In their modelling, the filtration phenomenon, i.e., changing in grout fluid density when it enters into a constriction, is reported as the most effective factor to stop grout fluid flow. However, only regular network of factures was considered in their study. Yang et al.[7] developed an analytical flow calculator in two-dimensional discrete fracture networks (DFN) in which the rheological equations governing the grout flow were used to obtain equivalent permeability tensors for the heterogeneous and anisotropic media. Shuttle and Glynn[8] also developed analytical method for a three-dimensional discrete fracture network. The Universal Discrete Element Code (UDEC) was utilized to analyze the fluid flow in a two dimensional network of fractures[9–13]. Equivalent permeability of the fractured rock mass is also estimated by conducting numerical analysis, and the effects of stress on the equivalent permeability were also considered in these studies. Finite element method (FEM) or extended FEM (XFEM) have been used[14–18] to simulate fluid flow in fractured rocks. However, applying these analytical and numerical methods for a large scale fractured media

* Corresponding author.
E-mail address: gwang@ust.hk (G. Wang).

http://dx.doi.org/10.1016/j.ijrmms.2017.07.015
Received 2 March 2017; Received in revised form 4 May 2017; Accepted 8 July 2017

is completely challenging due to their high computation cost, especially when geomechanical, chemical and temperature effects need to be considered. Therefore, some researches considered fractured rock as a continuum or hybrid-continuum media to solve the problem of upscaling of fluid flow[19,20], while the precision of the simulations for different scales might be variable. In engineering practice, three-dimensional flow properties are often deduced from two-dimensional calculations. Recently, Lang et al.[21] demonstrated that two-dimensional analysis cannot be directly used to approximate three-dimensional equivalent permeability of a fractured rock mass. However, some form of correction factor has been proposed to translate two- to three-dimensional permeabilities, at least at high fracture densities, when only two-dimensional analysis is available.

Most of previous literatures are unable to model various types of grout fluids, time-dependent phenomena such as grout hardening and/or influence of in-situ pore fluid. Most recently, Mohajerani et al.[22] developed a simple yet accurate numerical model to overcome some of the above limitations for predicting the grout propagation in the rock mass fractures, which is termed as Explicit Grout Forehead Pressure algorithm (EGFP). EGFP is a fully explicit algorithm for prediction of the grout penetration length in a pair of parallel slots using three types of parameters, including geometrical parameters of a single fracture, rheological parameters of grout fluid and operational parameters of grouting operation. EGFP was designed to consider the filtration phenomenon, time-dependent grout hardening and also the effects of gravity and in-situ pore fluid pressure. Furthermore, different types of grout fluid behavioral model (Newtonian, Bingham or power-law) could be modeled using the EGFP algorithm[22].

In order to simulate a practical grouting operation, it is necessary to generalize EGFP to a network of interconnected fractures modeled by Discrete Fracture Network (DFN). The DFN method was introduced in the late 1970s as "analysis and modelling in which explicitly involves the geometry of fractures, as the fundamental factor controls the fluid flow"[23]. The method uses Monte-Carlo simulation to generate fracture networks based on probability density functions (PDF) of geometric parameters of joint sets, which can be obtained from field surveys. Since the DFN method can incorporate field variation of joint distribution, grouting simulation based on the DFN can be more realistic compared with other methods.

The geometry of DFN simulation includes density, dip, dip direction and length of fracture sets as well as aperture of single fractures, which have important influence on the flow of the grout fluid. In many researches, it is usually assumed that the rock matrix is impermeable[24]. Fracture length usually is demonstrated by the power-law, log-normal or negative exponential distribution function. The distribution function of aperture is usually power-law or log-normal. Conductivity of fractures is related to the aperture through the cubic law and is determined from the in-situ data. It seems logical that the aperture and the length of the fractures are correlated. This relationship has been reported as power-law with linear or sublinear scaling[24]. Many different codes are developed to implement the DFN method. For example, a code to generate a two-dimensional network of discrete fractures has been developed[25]. In this code, geometric parameters of fractures include fracture position (derived from the joint density), orientation (including dip angle and dip direction), fracture length (a function of the fracture trace length), and fracture aperture.

2. Development of GrouIUT^{2D} program: generalizing EGFP algorithm to DFN

GroutIUT^{2D} is structurally divided into two main sections: two-dimensional DFN generation, and generalization of EGFP algorithm to this generated network. More discussion about these two sections is provided in the following.

2.1. DFN generation

A program module in C++ has been developed for generating DFN in GroutIUT2D. The generation procedure involves the following steps as described in[25,26]:

I. Specifying a generation domain and the number of DFN realizations.
II. Generating the locations of centers of fractures using Poisson's process, according to the measured fracture intensity for each joint set.
III. Generating fracture orientation, based on approximated PDF for each joint set.
IV. Generating trace length of fractures according to the approximated PDFs for each joint set.
V. Repeating steps (II) to (IV) for all sets of fractures using Monte-Carlo method. The random occurrence of discontinuities along a line is an instance of a one-dimensional Poisson process. A Poisson process is defined by assuming that any small increment along the line has the same, but very small, probability of containing a discontinuity occurrence. If the total discontinuity frequency is λ, it can be shown that the probability $P(k, x)$ of exactly k discontinuity intersections occurring in an interval of length x, selected at random along the line, is given by the following equation[27]:

$$P(k, x) = \frac{e^{\lambda x}(\lambda x)^k}{k!} \quad (1)$$

If discontinuity intersections along a line obey a one-dimensional Poisson process, then it is reasonable to assume that the occurrence of the mid-points of the discontinuity trace in a plane will obey a two-dimensional Poisson process[27].

The DFN module was further improved to better accommodate the EGFP algorithm. For example, boundaries were changed to conform with dimensions of grouting operation domain, and position of grouting wellbore was added and output matrix of position of fractures were rearranged.

2.2. The EGFP algorithm

The explicit grout forehead pressure (EGFP) algorithm has been developed to estimate grout penetration length in a single fracture[22]. This algorithm follows an explicit iterative scheme for estimating grout penetration length in a singular fracture. In this algorithm, the penetration length is determined using rheological equations of fluid through a pair of parallel slots. For simplicity, two walls of a fracture are simulated as an identical line with a given aperture and each fracture line is divided into a number of small segments. Geometrical parameters of the fracture, initial pressure of grout fluid and the maximum grouting duration time are the initial parameters given to the model. The stopping criteria for grout propagation are depletion of grout fluid forehead pressure and/or finishing of the considered maximum grouting duration time. These stopping criteria finally cease the movement of grout fluid forehead inside the fracture. Depletion of fluid pressure is due to the pressure drop caused by resistance of the pore fluid pressure, frictional effect, filtration phenomenon and grout hardening. The effect of gravity is depended on position of grout forehead and also the density of grout and pore fluid. Therefore, the gravity can be either a contributory or a disincentive factor for grout fluid flow[22].

The EGFP algorithm is schematically illustrated in Fig. 1. As shown in Fig. 1(a), the pairs of parallel slots are simplified to singles lines. The fracture 1 is intercepted by the grouting borehole and fracture 2 at nodes i and j, respectively. The EGFP algorithm is based on explicit calculation of grout flow in small computational segments formed on each fracture. Denote P_0 as the pressure in the grout forehead, and P_L as the pore fluid pressure within the facture. They are acting at two ends

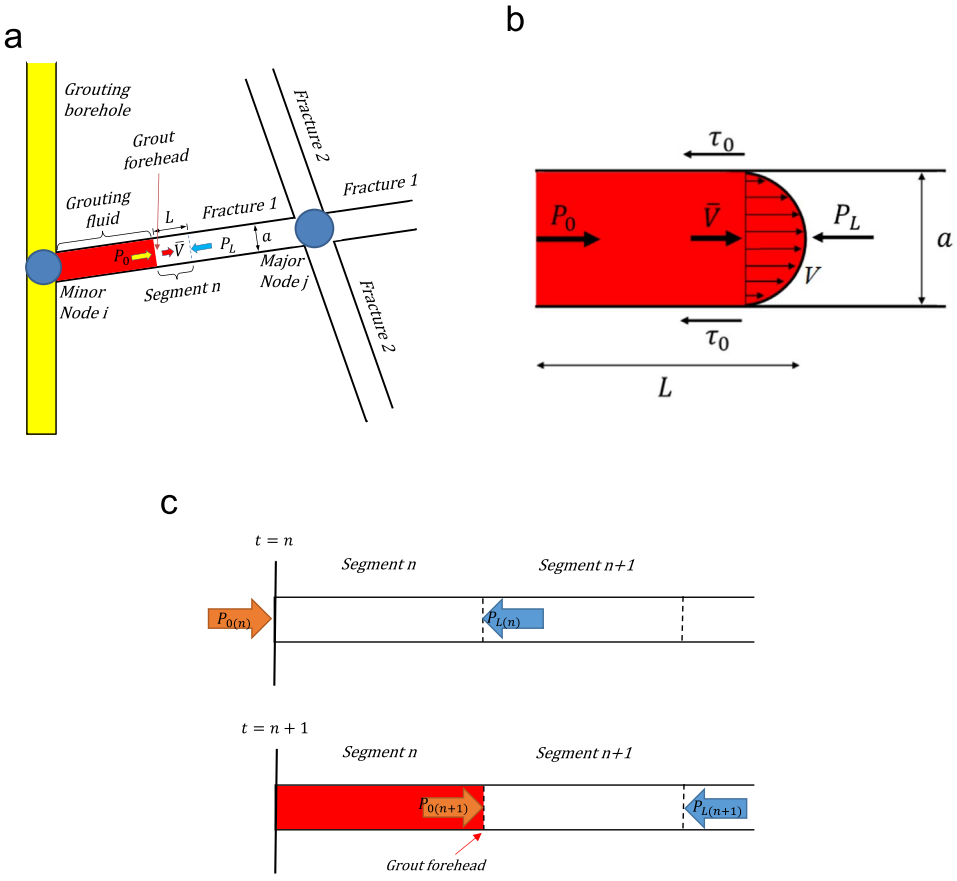

Fig. 1. (a) A scheme of grout forehead, joints, elements, nodes and grouting borehole. (b) a scheme of active forces on an element. (c) a scheme of propagation during consecutive time steps.

of the segment n, a is the effective hydraulic aperture, and L is the length of the segment. It is supposed that P_0 is known at the first segment of the fracture 1 as the boundary condition, and P_L is known everywhere.

As proposed by Barton et al.[28], the effective hydraulic aperture a can be related to physical aperture and joint roughness by an empirical model. On the other hand, indirect estimation of a can be obtained by measurement of the permeability of a rock mass[27]. By the parallel plate analogy (cubic law), an estimate for the average effective hydraulic aperture a can be obtained through the following equation:

$$a = \left[\frac{12\mu K_m}{\lambda\rho g}\right]^{1/3} \tag{2}$$

where K_m is the apparent mass permeability given by a flow test, g is the gravitational acceleration, ρ is the density of the fluid, μ is the dynamic viscosity, and λ is fracture frequency.

As shown in Fig. 1(b), the average velocity of the grouting fluid forehead propagating through the segment n can be determined by the pressure gradient and the properties of the grouting fluid. For a Bingham fluid, the grout forehead average velocity ($\bar{V}$) through a pair of parallel plates is given by Eq. (3)[22]:

$$\bar{V} = \frac{(P_0 - P_L)a^2}{12\mu L}\left\{1 - \frac{3\tau_0 L}{(P_0 - P_L)a} + 4\left[\frac{\tau_0 L}{(P_0 - P_L)a}\right]^3\right\} \tag{3}$$

Alternatively, the average grout forehead velocity of a power-law fluid is according to[22]

$$\bar{V} = \frac{a}{2 + (1/n)}\left[\frac{(P_0 - P_L)a}{2kL}\right]^{1/n} \tag{4}$$

where τ_0 is the initial yield stress of the Bingham fluid, n is the behavioral index of the power-law fluid and k is the consistency index of the power-law fluid.

As shown in Fig. 1(c), the grouting fluid will propagate into segment n by the average forehead velocity $\bar{V}$. Therefore, the grout fluid will fill in the segment at $t_{n+1} = t_n + L/\bar{V}$. Then, the pressure of the grout forehead drops from $P_{0(n)}$ at t_n to $P_{0(n+1)}$ at t_{n+1} through the following equation:

$$P_{0(n+1)} = P_{0(n)} - \Delta P_{total(n)}, \tag{5}$$

where $\Delta P_{total(n)}$ is the total resistant pressure and is obtained using Eq. (6).

$$\Delta P_{total(n)} = \Delta P_{l(n)} + \Delta P_{g(n)} \tag{6}$$

where $\Delta P_{l(n)}$ is frictional pressure drop and $\Delta P_{g(n)} = \rho g \Delta h$ is the pressure change due to difference in elevation (Δh) at two ends of the segment, where ρ is the density of the grout fluid. In particular, the frictional pressure drop can be determined by the forehead velocity $\bar{V}$ through Darcy-Weisbach equation[29]:

$$\Delta P_{l(n)} = \rho \cdot f_D \frac{l_e}{D_{he}} \frac{\bar{V}^2}{2}, \tag{7}$$

where, f_D, l_e and $D_{he}$are Darcy roughness coefficient, element length and equivalent hydraulic diameter of fracture, respectively. For flow between parallel plates, $D_{he} = 2a$, i.e. two times of the effective hydraulic aperture. Accordingly, f_D can be estimated based on the state of flow (laminar or turbulent) and the type of grout fluid (Bingham or power-law)[22].

Using an explicit iterative method, the calculated forehead pressure will be updated following Eq. (6) when the grout fluid propagates into a segment. The updated pressure will be used for grout propagation into

the next segment. Since the element length and average velocity of grout fluid is known, it is possible to calculate simply the grout passing time at each element. Therefore, the effect of time-dependent grout hardening can be considered by changing viscosity of the grout fluid. Also, the effects of filtration phenomenon, i.e. changing in grout fluid density when it enters into a constriction, can be modeled. The grout forehead continues to propagate until the stopping criteria are satisfied.

2.3. GroutIUT^{2D} development

The EGFP algorithm is developed to calculate time and penetration length of the grout fluid inside a single fracture. For a network of fractures, the influence of connectivity pattern of the network must be considered. When the grout fluid passes through a multi-way junction into branches, additional pressure drop must be included into Eq. (6) for the total pressure drop in the grout forehead. The additional pressure drop can be determined via Eq. (8) by assuming the grout fluid passes through a virtual fracture with an equivalent fracture length[29]:

$$L_{eq(n)} = \kappa . D_{he} \quad (8)$$

where $L_{eq(n)}$ is equivalent length of the virtual fracture, and D_{he} is the equivalent hydraulic diameter. κ is a constant coefficient depending on the type of the multi-way junction. In the program, κ is chosen as 15 and 50 for a 3-way and 4-way junction, respectively.

Note that the equivalent length is virtual, the grout propagation time through it will be set as zero. Correspondingly, the stopping point (also called the cut-off point) of the grout forehead never forms in the multi-way junction. If the farthest cut-off points from the grouting wellbore are connected together, they create a propagation surface. The propagation surface can be a key criterion for measuring the groutability in rock engineering projects such as determination of grouting wellbore spacing or estimation of sealing efficiency.

Fig. 2 illustrates the flowchart of GroutIUT^{2D} program. A graphical user interface (GUI) has been developed in GroutIUT^{2D} to visualize the DFN framework, grouting wellbore, pore fluid table line, initial and calculated parameters, and the grout propagation surface. Grouted fractures are displayed by the bold red lines.

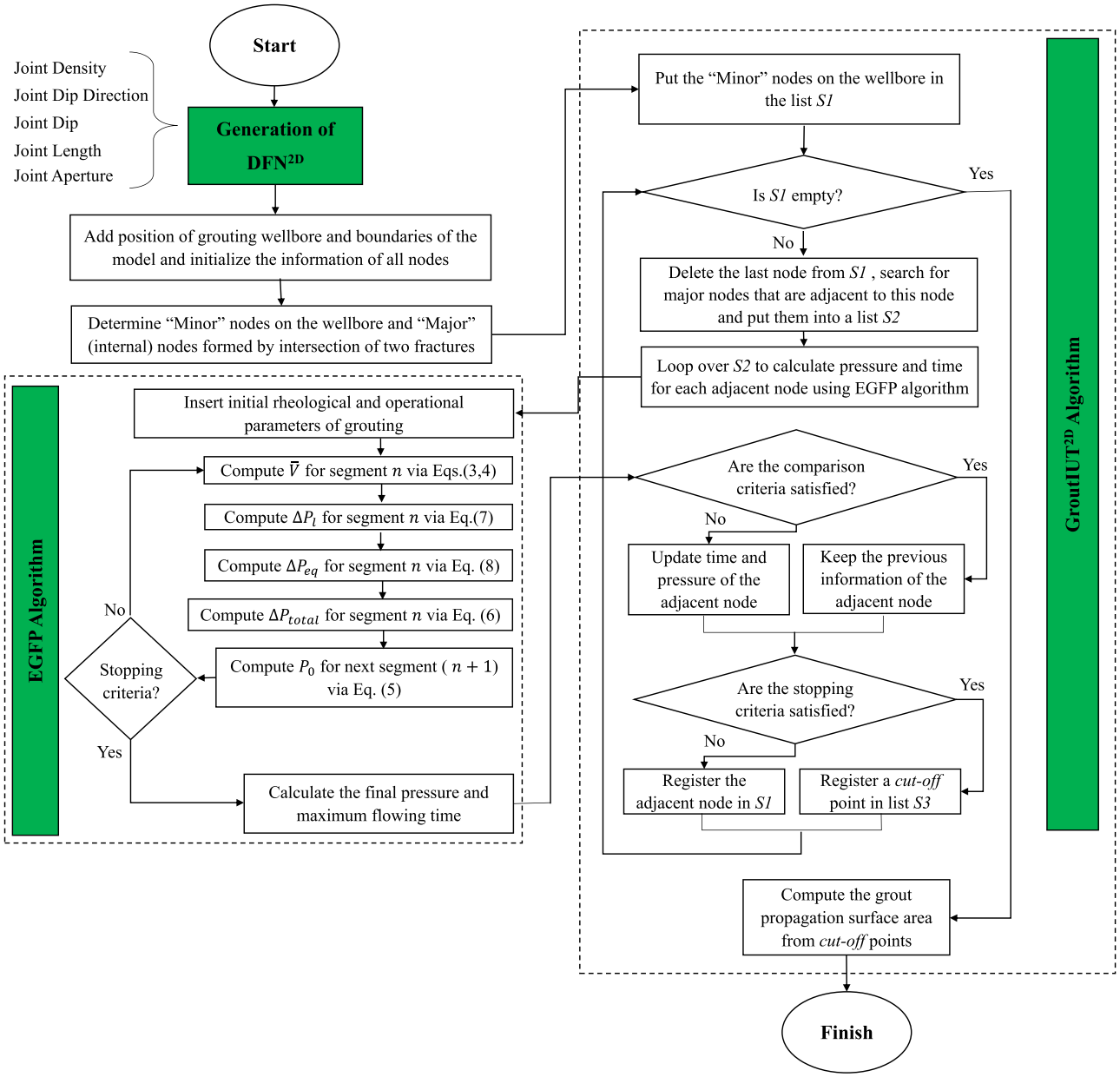

Fig. 2. The flowchart of GroutIUT^{2D} program.

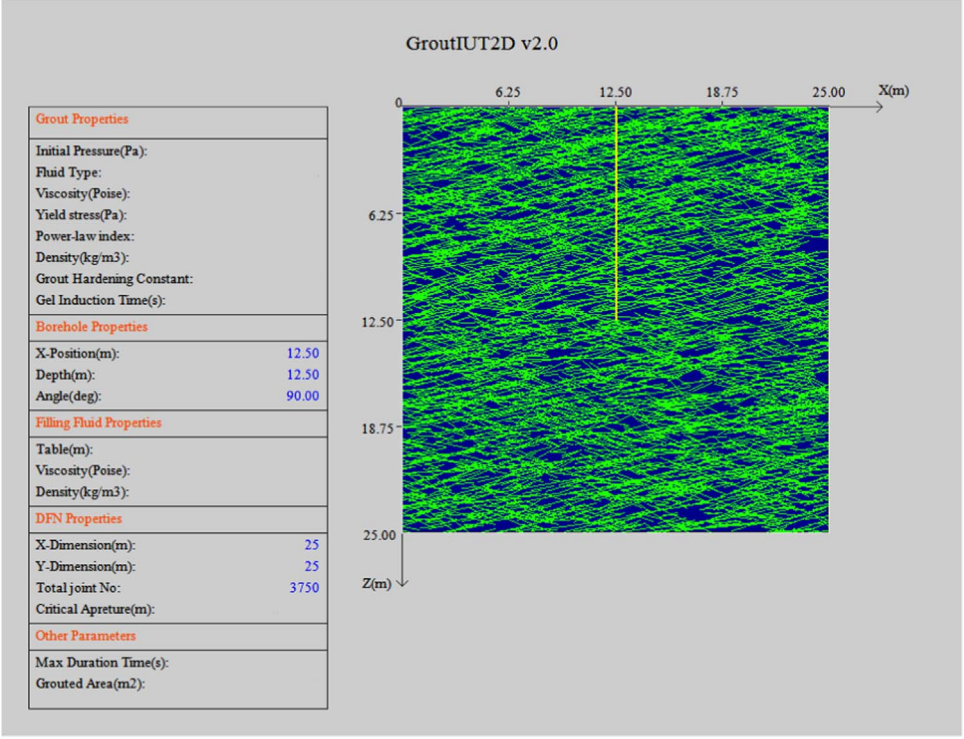

Fig. 3. A DFN realization with a wellbore generated by GroutIUT^{2D} program.

As shown in Fig. 3, DFN is simulated with a specified domain. This simulated DFN is one of the several random realizations created with the same geometrical and statistical parameters of jointed rock mass. GroutIUT^{2D} also prescribe the geometry of grouting wellbore in the simulation domain.

After identifying all the nodes in the desired domain, the program begins to remove the fractures so called “dead-end” or “isolated”. Isolated fractures which do not intersect with any other fractures or boundary line are not considered actually as a path for transmitting grout fluid and thus are removed. However, dead-end fractures are connected with the other fractures at only one end. It is assumed that the pore air / fluid is trapped in these fractures. Therefore, dead-end fractures will prevent the entrancing of the grout fluid forehead into themselves and should be removed from the domain for increasing speed of modelling.

Consider n_f is the total number of internal fractures in DFN. Since in this two-dimensional region there are four boundaries and one wellbore, the total number of linear elements form connectivity pattern is:

$$n_t = n_f + 5 \tag{9}$$

Any linear element is shown by F_i where $i \in 1, \ldots, n_t$. As previously mentioned, each node is formed by intersection of two fractures F_i, F_j. Therefore, a node is defined as: $\xi = \{\xi_k \mid F_i \bigcap F_j, i, j \in 1, \ldots, n_t, i \neq j\}$. Internal nodes formed by intersection of two fractures are called “major nodes”. The set of all major nodes is shown by $N \subset \xi$. By the way, n_N is the number of members of N. On the other hand, intersection of a fracture with the wellbore or the boundary box of the DFN is called a “minor node”. The set of all minor nodes and number of them are shown by $\lambda \subset \xi$ and n_λ, respectively. Therefore, the total number of nodes (members of ξ) is given by the Eq. (10).

$$n_T = n_n + n_\lambda \tag{10}$$

Information of each node includes its *ID* number (k), position (x, z), arrival time (the time when grout forehead location is on the node) (t) and corresponding grout forehead pressure (p). This information are in the form of set $\mathcal{L}_k = \{x_k, z_k, t_k, p_k\}$, $k = 1, \ldots, n_T$. The information of nodes is inserted in a two-dimensional matrix titled “connectivity matrix” ($\mathcal{M}_{ij}, i, j \in 1, \ldots, n_t$). The component $\mathcal{M}_{ij}$ is an empty set (ϕ) if $F_i \cap F_j = \phi$ (no intersection between two fractures), or $\mathcal{L}_k$ for information of the node formed by intersection of F_i and F_j. The adjacent nodes are a collection of nodes that are directly connected to node k in the fracture network. Since a node is an intersection of a maximum of two fractures, node k is able to have a maximum of four adjacent nodes.

According to Algorithm 1, $\mathcal{M}$ is updated in each iteration based on EGFP algorithm computation of p_k and t_k. At the first, GroutIUT^{2D} seeks around the grouting wellbore to find minor nodes λ and assigns values of $\mathcal{L}_k$ to $\mathcal{M}$ for each of these nodes based on the initial pressure (p_0) and time ($t_0 = 0$) in the wellbore. Consider $\mathcal{M}_{ij}^{(n)}$ is connectivity matrix for n^{th} iteration. Therefore, $\mathcal{M}_{ij}^{(0)}$ includes $\mathcal{L}$ for the wellbore nodes, and $\mathcal{M}_{ij}^{(1)}$ only includes updated $\mathcal{L}$ of the first wellbore node. The iterations continue to form complete connectivity matrix $\mathcal{M}$ with information of all of nodes in the domain. After all of the cut-off points are determined and are put in $S3$, it is time to estimate the grout propagation surface. A computational sub-code is merged in the GroutIUT^{2D} for calculating the closed surface area resulting from connecting outermost flow cut-off points inside the model around the grouting wellbore.

Fig. 4 illustrates grout propagation following the GroutIUT^{2D} algorithm. The fracture network consists of seven nodes. Nodes 1 and 5 are minor nodes, the remaining nodes are major nodes. As shown in Fig. 4(a), the calculation starts with node 1 to its only adjacent major node 2. Node 2 has three other adjacent nodes in the order of no. 4, 7 and 3. The information set (p_k and t_k) of $\mathcal{L}_k$ is then calculated for node 4 and 3 (k = 3,4). A cut-off point 1 is formed between nodes 2 and 7 when a stopping criterion (Algorithm 1(6)) is satisfied; Accordingly, the information for node 7 will not be updated, and node 7 will not be further considered in subsequent calculation. Then, consider grout propagation from node 3 to its only adjacent node 6. When a stopping criterion is satisfied, a cut-off point 2 is formed between nodes 3 and 6. Finally, consider grout propagation from node 4 to its adjacent nodes. Cut-off points 3 and 4 are formed in two (green) branches due to the comparison criteria and stopping criteria.

Fig. 4(b) illustrates the grout propagation routes starts from node 5. New information set for node 4 is obtained in this round of calculation,

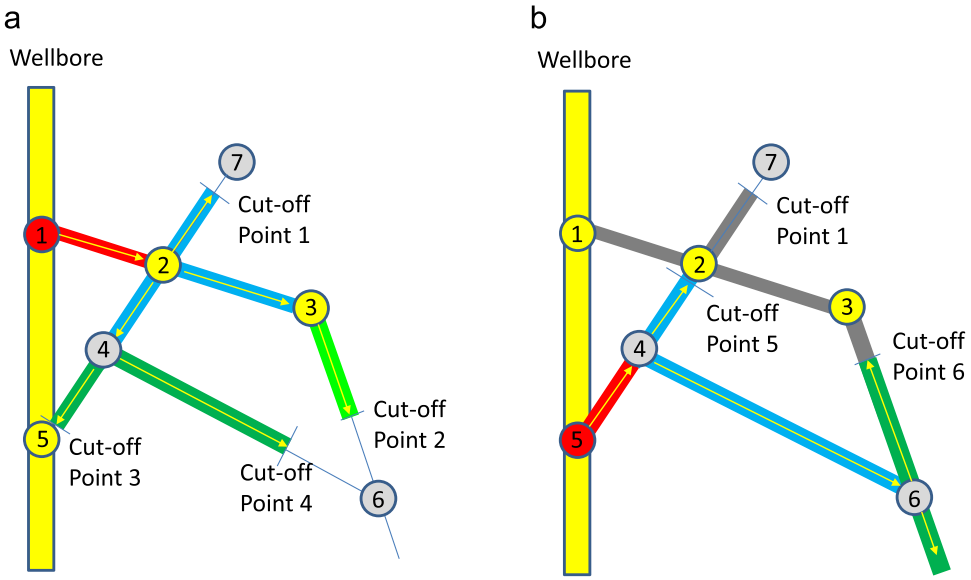

Fig. 4. Illustration of grout propagation using GroutIUT^{2D} algorithm.

which replaces the previous information of node 4 due to comparison criteria (Algorithm 1(5)). Cut-off point 4 is removed because grout propagates from node 4–6 for this case. At last, a cut-off point 6 is formed between nodes 6 and 3 when the time or pressure is depleted.

Algorithm 1. GroutIUT^{2D} algorithm for grout propagation.

(1) Initialize $t = 0$, $p = p_l$ for major nodes.
(2) Find all minor nodes k, and updated their $\mathcal{L}_k$ on $\mathcal{M}$. Put node ID k into a list ($S1$).
(3) If $S1 \neq \phi$, Select the last node (α) in the list, delete it from the list and search for its adjacent nodes based on matrix $\mathcal{M}$. Put all of adjacent nodes in a list ($S2$) and got to 4.
Otherwise, go to 7.

(4) If $S2 \neq \phi$, Select the last node (β) in the list $S2$, delete it from the list $S2$ and go to 5.
Otherwise, go to 3.
(5) [*Comparison criteria*] Consider t_1 and p_1 are initial time and initial pressure of node β, respectively. Compute $t_2$and p_2 of β according to EGFP algorithm.
If $t_2 > t_1$ and $p_2 < p_1$ (the criteria are satisfied), keep $\mathcal{L}_\beta$ on $\mathcal{M}$ for node β as $\{t_1, p_1, x, z\}$. Form the *cut-off* point and put it at a list ($S3$);
Otherwise, update $\mathcal{L}_\beta$ on $\mathcal{M}$ for node β as $\{t_2, p_2, x, z\}$.
(6) [*Stopping criteria*] If $t > t_{max}$ or $p_0 \leq p_l$ (the criteria are satified), form the *cut-off* point and put it at a list ($S3$) and go back to 3;
Otherwise, put *ID* of β into the list ($S1$) and go back to 4.
(7) End.

Using GroutIUT^{2D} algorithm, Fig. 5 shows grout propagation patterns in a 25 m × 25 m DFN domain. The number of joint sets, type of PDF and value of statistical parameters of density, dip direction, dip, length and aperture of DFN fractures are given in columns 1 - 6 of Table 1, respectively. The grout fluid is a Bingham fluid with time-dependent hardening of grout fluid viscosity specified using the following equation[22,30]:

$$\mu = \mu_0\{1 + \exp[\xi_g(t/t_g - 1)]\} \quad (11)$$

where μ_0 is the initial gout viscosity, ξ_g is a grout hardening constant. As grout develops to a gel after a given time interval, the gel induction time t_g corresponds to the time interval in which viscosity of the grout increases to two times of its initial value[30]. Finally, parameters of the grout fluid are specified as follows: μ_0 is 0.1 poise, density is 1500 kg/m^3, initial yield stress is 2 Pa, grout hardening constant ξ_g is 1.5, and gel induction time t_g is 1800 s.

3. Model validation

In this research, two series of laboratory tests performed by[31,32] have been used to validate the GroutIUT^{2D} program. Previously, the EGFP algorithm has been successfully validated for a single fracture by experimental results[22]. Therefore, only for understanding the concept of generalization of EGFP to a network of fractures and validation of the results, a number of simple lattice networks have been considered.

3.1. Experiment 1

As shown in Fig. 6(a), the experimental set-up consists of two plates of plexiglass with the dimensions of 1.2 × 1 × 0.015 m. A lattice channel network has been constructed by placing rectangular cubes of plexiglass in a symmetrical pattern between the two plates forming 1 × 5 mm channels. The construction has been placed at a small angle to the horizontal plane to construct a hydraulic gradient ($0.02m/m$). The construction has been injected with a grout fluid via its central node with an injection head of $0.48m$. The grout fluid had time constant properties and the rheological properties. The evaluated parameters were 3.0 Pa in yield value and 0.35 Poise in viscosity. The results from the laboratory experiment have been taken at different times after the start of injection and compared with the simulated propagation at those times[31].

3.2. Experiment 2

The laboratory set-up has been illustrated in Fig. 6(b). From the container the grout is injected to the actual set-up consisting of a network of pipes of different diameters. At the other end of the network the pipes are open. The network was constructed of pipes connected to each other. As shown in Fig. 6(c), pipes of three different radii (0.29 mm, 0.43 mm and 0.89 mm) have been used in the network. Two different grout fluid have been used in the experiment. The rheological parameters of grout fluid 1 are: the initial yield stress is 1 Pa, initial viscosity is 0.7 Poise, critical diameter for filtration phenomenon is 898 μm. The same parameters for grout fluid 2 are 1.3 Pa, 1.2 Poise and 110 μm, respectively[32]. Three tests were conducted in Experiment 2: test No. 1 and test No. 2 used fluid 1 and fluid 2 under injection pressure of 100 kPa, respectively, while test No. 3 used fluid 1 under injection pressure of 50 kPa[32].

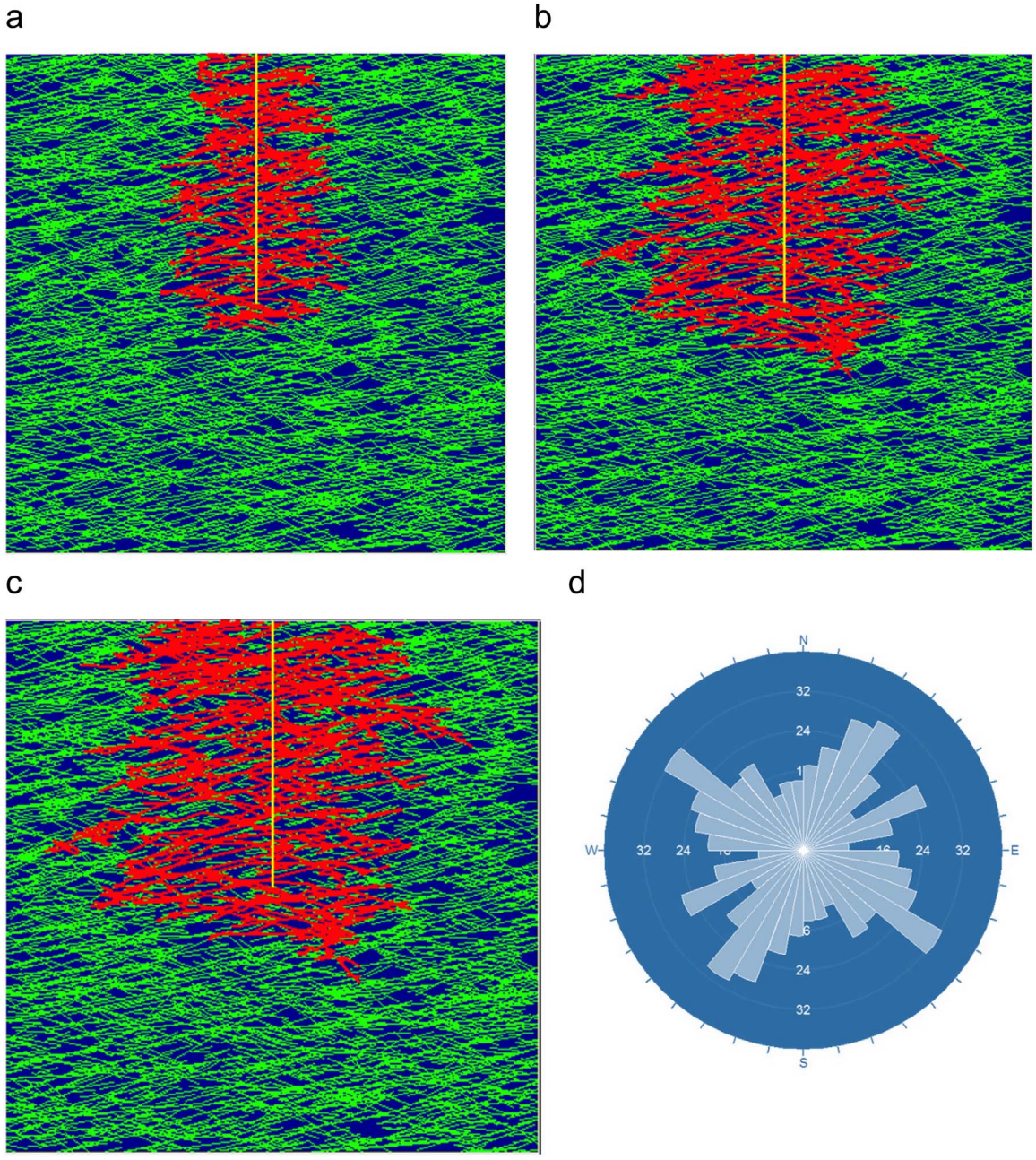

Fig. 5. A grouting process simulated in a 25 m × 25 m domain of DFN^{2D} using GroutIUT^{2D} program. operation time and initial pressure are (a) 60 s at 50 kPa, (b) 300 s at 50 kPa (c) 300 s at 100 kPa, respectively. (d) a rose diagram of mapped joints.

3.3. Comparison

GroutIUT^{2D} simulations have been carried out in such a way that a direct comparison between experiments and simulations could be performed. Due to the symmetry, only a half or a quarter of the model is modeled. Fig. 7 shows the visual comparison between the simulated and experimental results. More comparison between GroutIUT^{2D} simulations and laboratory experiments are provided in Fig. 8.

Fig. 8(a) compares results of experiment 1 with the GroutIUT^{2D} simulation at 2.5, 6, 22, 65 and 1400 s. The simulated propagation surface closely matches the experimental data. The simulation also indicates that the propagation surface starts to get stabilized after

Table 1
The geometrical / statistical parameters of the generated discrete fracture network.

Number of joint sets	Density of fractures (1/ m^2)	Fracture dip direction (Deg)	Average fracture dip (Deg) / Fisher constant	Average fracture length (m)/ Fractal dimension	Fracture aperture (mm)
1	2	43.55	84.29 / 22.57	20.00 / 1.78	0.15
2	2	131.60	84.99 / 13.75	20.00 / 1.78	0.15
3	2	246.30	38.10 / 14.30	20.00 / 1.78	0.15
PDF	Uniform	Poisson	Fisher	Power-law	Poisson

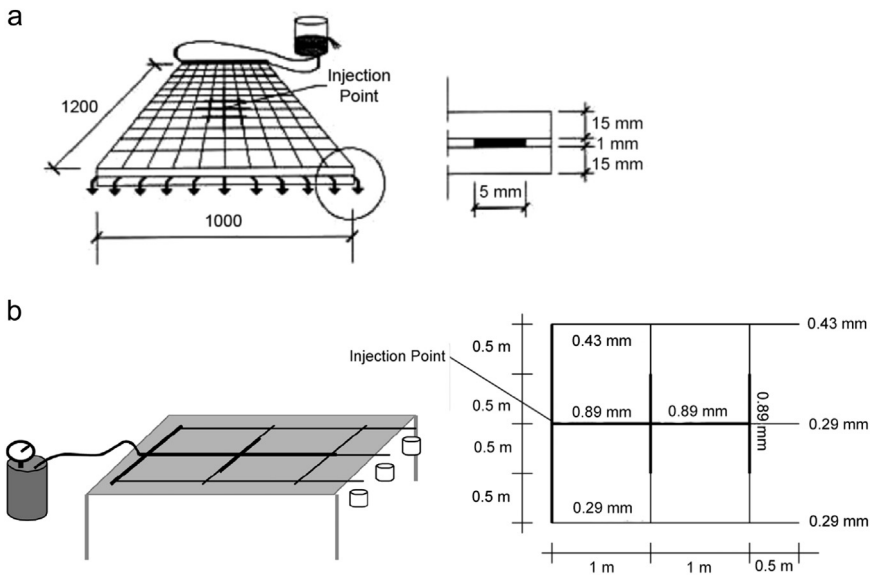

Fig. 6. (a) A schematic illustration of experimental set-up[29]. The channel cross section is visible in the right part of the figure. (b) A schematic illustration of laboratory test[30] with pipe radii and lengths in the network.

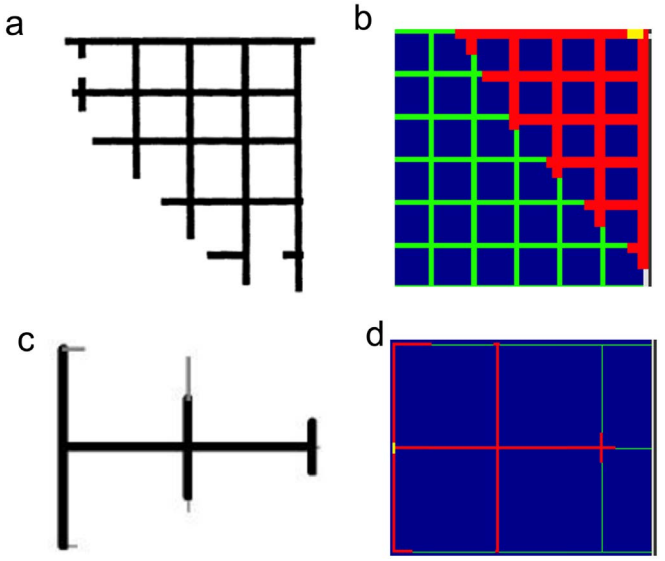

Fig. 7. Visual comparison between experiment results and GroutIUT^{2D} simulations. (a) Experiment 1 result for 65 s (b) Simulated result for experiment 1 for 65 s (c) Experiment 2 no 1 result for 20 s (d) Simulated result for experiment 2 no 1 for 20 s.

1000 s Fig. 8(b-d) compare three tests in experiment 2 with GroutIUT^{2D} simulations. All experiment data were sampled at 5, 10 and 20 s. Again, evolution of grout propagation surface predicted by GroutIUT^{2D} closely matches that of the experiment, except for small deviation in test No. 2.

All these benchmark examples validated the accuracy of the GroutIUT^{2D} simulations. In the followings, sensitivity analysis will be performed by the GroutIUT^{2D} to study the influence of model parameters.

4. Sensitivity analyses and discussions

Sensitivity analyses are performed in this session to study the influence of model parameters on grout propagation. In each analysis, only one parameter varies within a specified range, while all others remain to be constants.

The constant parameters include the operation time, the initial yield stress, the grout fluid density, initial viscosity and initial pressure are 600 s, 2 Pa, 1500 kg/m^3, 0.1 Poise and 25 kPa, respectively. Also, time-dependent hardening of grout fluid is deactivated. The grout fluid is cement-based and can be described by the Bingham rheological behavioral model. Geometrical/statistical properties of fractures are already listed in Table 1. It should be noted that the simulated grout propagation surface is resulted from arithmetic average over 10 different realizations of discrete fracture networks generated using the same group of parameters. The uncertainty in numerical simulations is clearly illustrated using error bars showing the arithmetic average plus/minus one standard deviation in each figure. In general, uncertainty associated with random realization of DFN is not pronounced. For many simulations, the coefficient of variation is just around 0.05–0.1.

The sensitivity analyses are carried out for both dry and saturated conditions for all varying parameters. In the dry and saturated conditions, the pore fluids are air and water respectively. As shown in Fig. 9, increasing density of cement-based grout fluid will increase the propagation surface for both dry and saturated conditions. For the saturated case, in-situ fluid pore pressure counteracts the grout propagation. It is only when grout density is greater than 1500 kg/m^3 that the expansion rate of the grout propagation surface significantly increases. The observed phenomenon should be related to increase in grout energy with increase in the grout density. Also, gravity helps increase propagation surface as the density of the grout becomes greater than that of the in-situ fluid. Therefore, it is advised to use heavier grout in the saturated case. On the other hand, the expansion rate of the grout propagation remains rather linear with increase in grout density in the dry case.

Fig. 10 shows the effect of initial grouting pressure on the propagation surface in both conditions. For the dry case, the propagation surface increases almost linearly with increase in the initial grouting pressure. For the saturated case, the rate of increase in the propagation surface becomes significant when the initial pressure is greater than a threshold value of about 25–50 kPa. The phenomenon is similar to the previous discussion: it seems that a threshold grout energy is required to break out the resistance of in-situ fluid pressure to gain a fast increase in expansion rate of the propagation surface.

The operation time of grouting is an important factor in grouting operation, which is determined by the user. The variation of operation time versus the grout propagation surface in the dry and saturated conditions are examined in Fig. 11. In both cases, the grout propagation surface increases with time to a limiting value. The corresponding

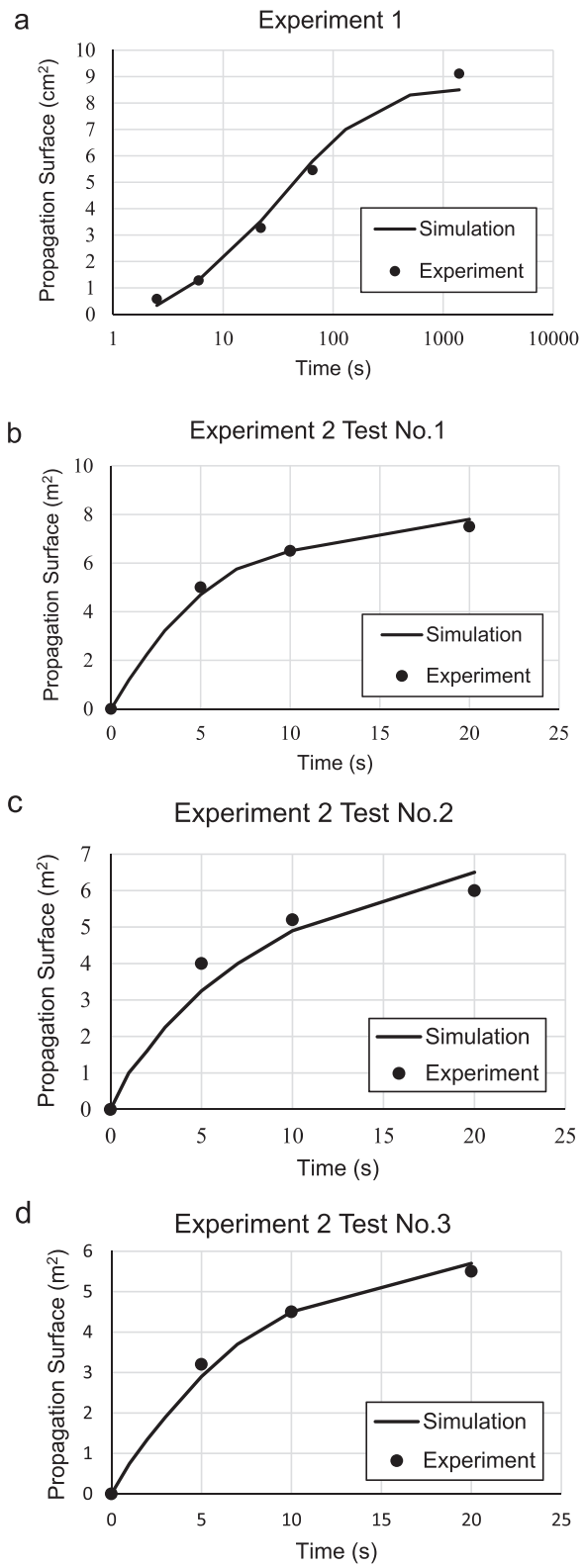

Fig. 8. Comparison between GroutIUT[2D] simulations and the results of (a) experiment 1, (b) experiment 2, test No.1, (c) experiment 2, test No.2, (d) experiment 2, test No.3.

operation time is called “critical time”. Beyond the critical time, the change in the propagation surface is negligible. For example, increasing the operation time from 2400 s to 4800 s only results in an increase in the grout surface area by 2–4%. Therefore, determination of the critical time could be useful to avoid the waste of money and time in a real grouting operation.

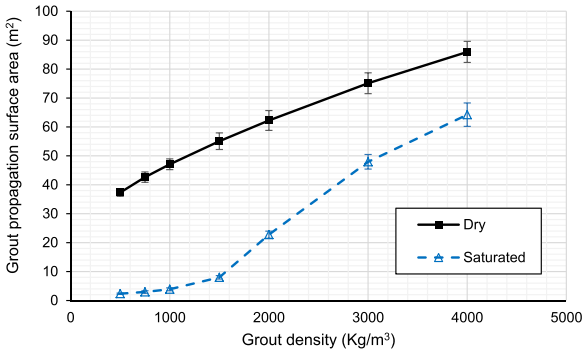

Fig. 9. the variation of density of grout fluid versus the grout propagation surface.

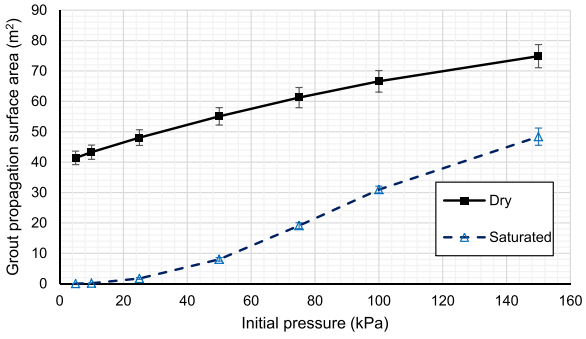

Fig. 10. The variation of initial grout pressure versus the grout propagation surface.

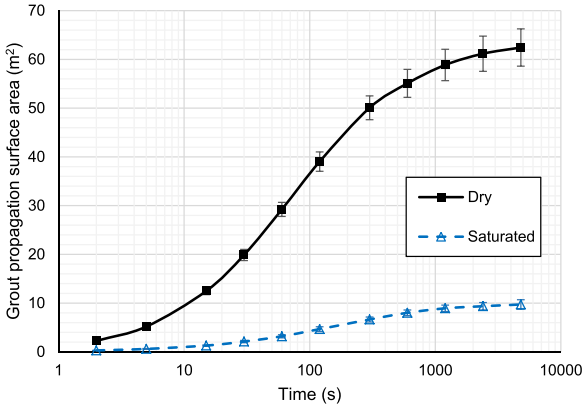

Fig. 11. The variation of operation time versus the grout propagation surface.

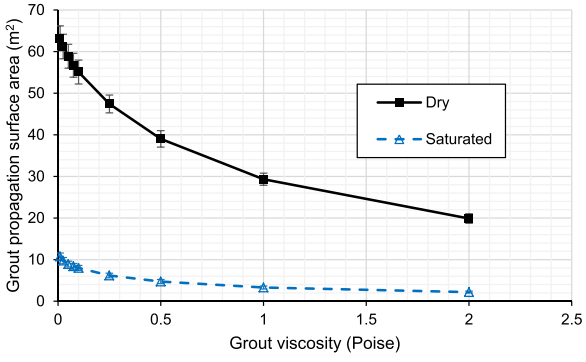

Fig. 12. The variation of grout fluid viscosity versus the grout propagation surface.

As seen in the Fig. 12, the grout propagation surface decreases with increasing grout viscosity. For the Bingham fluid, increase in fluid viscosity at a constant initial pressure causes decrease in fluid velocity and fluid kinetic energy consequently. The percentage of reduction in the propagation surface becomes significant when the grout fluid

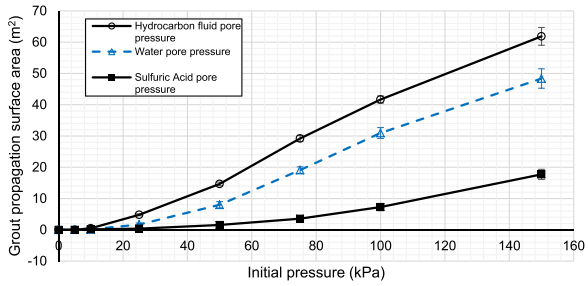

Fig. 13. The variation of initial grout pressure versus the grout propagation surface for three different pore fluid.

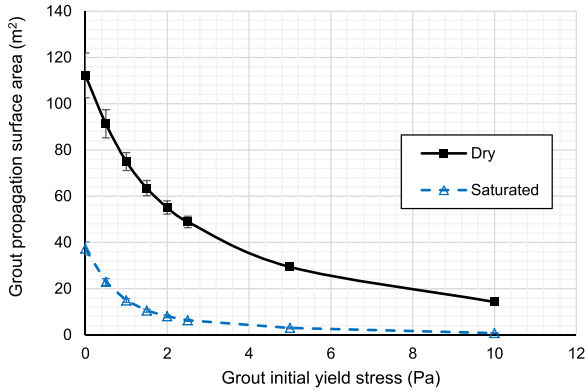

Fig. 14. The variation of initial yield stress versus the grout propagation surface.

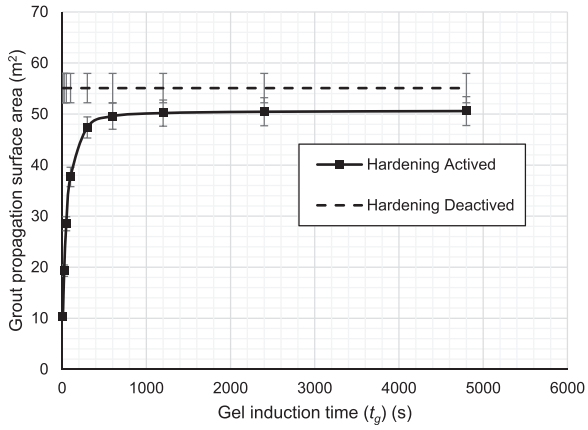

Fig. 15. The variation of gel induction time (t_g) versus the grout propagation surface.

viscosity is greater than 0.1 (Poise), which is defined as "critical viscosity" accordingly.

In order to assess the effect of in-situ pore fluid properties (viscosity and density), three simulations are compared in Fig. 13. In each simulation, the model is saturated by a different pore fluid, namely, water, hydrocarbon fluid and sulfuric acid. Hydrocarbon fluid was modeled as a Newtonian fluid with viscosity 0.09 Poise and density 850 kg/m^3, and sulfuric acid was modeled as a Newtonian fluid with viscosity 0.24 Poise and density 1840 kg/m^3. For reference, the viscosity of water is 0.01 Poise and density is 1000 kg/m^3. As shown in Fig. 13, the trend of the results seems vary significantly for different pore fluids. The grout propagation surface in sulfuric acid is the smallest due to high viscosity and high density of the fluid.

As pointed out before, the grout fluid used in the present sensitivity analysis is a Bingham fluid. Therefore, initial yield stress of the grout might also affect the groutability of the model. According to Fig. 14, the grout propagation surface decreases significantly with increase in the initial yield stress of the grout fluid. The reason for this trend is similar to that explained for fluid viscosity.

Fig. 15 shows the propagation surface versus gel induction time of the grout fluid, as is also compared with the upper-bound case when hardening is deactivated. Based on these analyses, the grout propagation surface area would not be much affected if gel induction time is longer than 600 s.

5. Conclusions

Simulation of grout propagation in a realistic fracture network is an important yet challenging problem in rock engineering. In the past, only limited experimental studies have been conducted on simple fracture networks. Although some empirical equations have been developed to predict groutability indicators, such as the grout penetration length given initial conditions, they were calibrated only by very limited amount of data and cannot be reliably generalized for practical usage. Therefore, an efficient computer algorithm is much needed to simulate the grout propagation with changing operational and rheological parameters.

GroutIUT^{2D} is such a program that takes advantage of recent development in Grout Forehead Pressure (EGFP) algorithm and generalizes it to two–dimensional discrete fracture networks (DFN). The EGFP algorithm can effectively predict the pressure and the propagation velocity of the grout forehead, making it a fast and accurate algorithm for predicting grout penetration in a single fracture. Furthermore, the effects of the time on grout properties and filtration phenomena can be easily incorporated in the EGFP algorithm.

An innovative grout propagation algorithm is then developed in GroutIUT^{2D} to generalize the EGFP to DFN. The algorithm employs a recursive scheme to track the paths of grout propagation within the fractures. The grout stops propagating when the forehead pressure is depleted. The GroutIUT^{2D} algorithm has been successfully validated using two series of laboratory tests.

Sensitivity analyses have also been performed to study the influence of model parameters. For both dry and saturated in-situ conditions, the grout propagation surface generally increases with increase in grout density, initial pressure and operation time. The influence of grout fluid viscosity and initial yield stress are also studied. Through the analyses, critical time and critical viscosity are quantified, which provides very useful information for the efficiency of the grouting operation. The program is also capable of investigating some less studied factors, including rheology properties of the in-situ pore fluid, time-dependent hardening and initial yield stress of the grout fluid. These factors are also found to be important for improving efficiency of the grout operation.

It is also noted that due to computational limitations and simplicity, current study is only limited to two-dimensional analysis. Yet, the algorithm has great potential to be extended to a three-dimensional DFN, which will the focus of our future study. Similar to Liang et al.[21], a correction model that translates calculations of grout propagation from two-dimensional to three-dimensional analysis can be explored in the future.

Acknowledgements

SM acknowledges financial support jointly from Ministry of Science, Research and Technology of Iran and HKUST, and GW is supported by Hong Kong Research Grants Council TBRS grant no. T22-603-15N. Any opinions, findings, and conclusions or recommendations expressed in this paper are those of the authors and do not necessarily reflect the view of the sponsors and other individuals.

References

1. Gustafson G, Stille H. Prediction of groutability from grout properties and hydrogeological data. *Tunn Undergr Space Technol*. 1996;11(3):325–332.
2. Hernqvist L, Fransson Å., Gustafson G, Emmelin A, Eriksson M, Stille H. Analyses of the grouting results for a section of the APSE tunnel at Äspö hard rock laboratory.

Int J Rock Mech Min Sci. 2009;46(3):439–449.
3. Fransson Å., Gustafson G. The use of transmissivity data from the probe holes for predicting tunnel grouting: analyses of data from the access tunnel to the Äspö hard rock laboratory. *Tunn Undergr Space Technol.* 2000;15(4):365–368.
4. Eriksson M, Stille H. A method for measuring and evaluating the penetrability of groutsJohnsen LF, Bruce DA, Byle MJ, eds. Grouting and ground treatment, Reston VA: ASCE; 2003, pp.1326–1337.
5. Wang M, Kulatilake PH, Um J, Narvaiz J. Estimation of REV size and three-dimensional hydraulic conductivity tensor for a fractured rock mass through a single well packer test and discrete fracture fluid flow modeling. *Int J Rock Mech Min Sci.* 2002;39(7):887–904.
6. Eriksson M, Stille H, Andersson J. Numerical calculations for prediction of grout spread with account for filtration and varying aperture. *Tunn Undergr Space Technol.* 2000;15(4):353–364.
7. Yang MJ, Yue ZQ, Lee PK, Su B, Tham LG. Prediction of grout penetration in fractured rocks by numerical simulation. *Can Geotech J.* 2002 1;39(6):1384–1394.
8. Shuttle DA, Glynn E. Grout curtain effectiveness in fractured rock by the discrete feature network approachJohnsen LF, Bruce DA, Byle MJ, eds. Grouting and ground treatment, Reston, VA: ASCE; 2003, pp.1405–1416.
9. Saeidi O, Stille H, Torabi SR. Numerical and analytical analyses of the effects of different joint and grout properties on the rock mass groutability. *Tunn Undergr Space Technol.* 2013;38:11–25.
10. Min KB, Rutqvist J, Tsang CF, Jing L. Stress-dependent permeability of fractured rock masses: a numerical study. *Int J Rock Mech Min Sci.* 2004;41(7):1191–1210.
11. Zhang X, Sanderson DJ, Harkness RM, Last NC. Evaluation of the 2-D permeability tensor for fractured rock masses. *Int J Rock Mech Min Sci Geomech Abstr.* 1996;33(1):17–37.
12. Liao QH, Hencher SR. Numerical modelling of the hydro-mechanical behaviour of fractured rock masses. *Int J Rock Mech Min Sci.* 1997;34(3–4) [177.e1-e17].
13. Baghbanan A, Jing L. Stress effects on permeability in a fractured rock mass with correlated fracture length and aperture. *Int J Rock Mech Min Sci.* 2008;45(8):1320–1334.
14. Huyakorn PS, Lester BH, Faust CR. Finite element techniques for modeling groundwater flow in fractured aquifers. *Water Resour Res.* 1983;19(4):1019–1035.
15. Baca RG, Arnett RC, Langford DW. Modelling fluid flow in fractured porous rock masses by finite element techniques. *Int J Numer Methods Fluids.* 1984;4(4):337–348.
16. Zhang J, Standifird WB, Roegiers JC, Zhang Y. Stress-dependent fluid flow and permeability in fractured media: from lab experiments to engineering applications. *J Rock Mech Eng.* 2007;40(1):3–21.
17. Zhang QH, Yin JM. Solution of two key issues in arbitrary three-dimensional discrete fracture network flow models. *J Hydrol.* 2014;514:281–296.
18. Prevost JH, Sukumar N. Faults simulations for three-dimensional reservoir-geo-mechanical models with the extended finite element method. *J Mech Phys Solids.* 2016;86:1–8.
19. Gan Q, Elsworth D. A continuum model for coupled stress and fluid flow in discrete fracture networks. *Geomech Geophys Geo-Energy Geo-Resour.* 2016;2(1):43–61.
20. Kumar A, Camilleri D, Brewer M. Comparative analysis of dual continuum and discrete fracture simulation approaches to model fluid flow in naturally fractured, low-permeability reservoirs. In: *Proceedings of SPE low perm symposium.* Denver, Colorado; 5-6 May; 2016.
21. Lang PS, Paluszny A, Zimmerman RW. Permeability tensor of three-dimensional fractured porous rock and a comparison to trace map predictions. *J Geophys Res Solid Earth.* 2014;119(8):6288–6307.
22. Mohajerani S, Baghbanan A, Bagherpour R, Hashemolhosseini H. Grout penetration in fractured rock mass using a new developed explicit algorithm. *Int J Rock Mech Min Sci.* 2015;80:412–417.
23. Dershowitz WS, La Pointe PR, Doe TW. Advances in discrete fracture network modeling. In: *Proceedings of the US EPA/NGWA fractured rock conference.* Portland, Maine; 2004; 13-15 September. 2004. p. 882-894.
24. Lei Q, Latham JP, Tsang CF. The use of discrete fracture networks for modelling coupled geomechanical and hydrological behaviour of fractured rocks. *Comput Geotechnol.* 2017;85:151–176.
25. Baghbanan A, Joolaei A. The generation of 2D and 3D stochastic fracture networks. In: *Proceedings of the 14th symposium of geological society of Iran.* Urmia, Iran. 2010. p. 1-6.
26. Jing L, Stephansson O. Discrete element methods for granular materials. *Dev Geotech Eng.* 2007;85:399–444.
27. Priest SD. Discontinuity analysis for rock engineering, Netherlands: Springer Science & Business Media; 2012.
28. Barton N, Bandis S, Bakhtar K. Strength, deformation and conductivity coupling of rock fractures. *Int J Rock Mech Min Sci.* 1985;22:121–140.
29. Schaschke C. Fluid mechanics: worked example for engineers, Rugby, Warwickshire, UK: The Institution of Chemical Engineers; 2005.
30. Funehag J, Gustafson G. Design of grouting with silica sol in hard rock – New methods for calculation of penetration length, Part I. *Tunn Undergr Space Technol.* 2008;23(1):1–8.
31. Håkansson U. Modellförsök – Icke-Newtonsk strömning i endimensionella kanaler [Master Thesis], Stockholm, Sweden: Department of Civil and Environmental Engineering, KTH Royal Institute of Technology; 1987.
32. Eriksson M. Prediction of grout spread and sealing effect Ph.D. Thesis, Stockholm, Sweden: Department of Civil and Architectural Engineering, KTH Royal Institute of Technology; 2002.